POLITECNICO
MILANO 1863

SCUOLA DI INGEGNERIA INDUSTRIALE
E DELL'INFORMAZIONE

Executive Summary of the Thesis

Characterization and Corrosion Performance of Chromium-Based Bilayer Coatings for Lead-Cooled Fast Reactors

Laurea Magistrale in Nuclear Engineering - Ingegneria Nucleare

Author: Marco Libera

Advisor: Prof. Valeria Russo

Co-advisor: Laura Sanna

Academic year: 2025-2026

---

1. Introduction

The transition towards clean and sustainable energy has placed Generation IV nuclear systems, particularly Lead-Cooled Fast Reactors (LFRs), at the forefront of advanced power generation. LFRs offer enhanced passive safety features, superior thermal efficiency, and the ability to operate with a closed fuel cycle, which significantly reduces long-lived radioactive waste. However, the commercial deployment of these reactors is currently hindered by severe material compatibility challenges. At operating temperatures exceeding 500 °C, the heavy liquid metal coolant acts as a highly aggressive environment, subjecting structural components to severe Liquid Metal Corrosion (LMC), dissolution, oxidation, and Liquid Metal Embrittlement (LME). To overcome these critical bottlenecks, the application of protective coatings on structural components has emerged as the most viable near-term mitigation strategy [1].

Chromium is an established material for anticorrosive applications in harsh environments. Its exceptional protective capability stems from a high affinity for oxygen, enabling it to spontaneously develop a dense, robust, and passivating Cr_2O_3 (chromia) scale in oxygen-containing environments. The deposition of pure metallic chromium thin films has been widely investigated for the production of Accident Tolerant Fuels (ATFs) to improve the resilience of conventional Light Water Reactors (LWRs). Indeed, numerous studies over the past decade have confirmed the effectiveness of chromium coatings in enhancing the degradation resistance of LWR fuel elements [2]. Furthermore, since the overall efficacy of these coatings is intrinsically linked to the synthesis technique, High-Power Impulse Magnetron Sputtering (HiPIMS) was selected as the most suitable deposition technique for the production of highly compact, firmly adherent, and structurally homogeneous metallic films that are highly resistant to crack propagation [2].

Given these properties, metallic chromium-based coatings represent a highly promising solution for LFR applications [3]. Nevertheless, the current literature lacks comprehensive data regarding both the fundamental high-temperature oxidation kinetics of these specific films and their efficacy in mitigating corrosion during prolonged exposure to liquid lead.

1.1. Thesis Objectives

To fill this research gap, this thesis aims to systematically characterize the oxidation behavior of HiPIMS-deposited chromium thin films and evaluate their efficacy as anticorrosive barriers for LFR applications. The first half of the study focuses on the fundamental structural evolution of the metallic films, evaluating how controlled thermal oxidation in air promotes the growth of dense Cr_2O_3 scales. This fundamental material characterization was then exploited to engineer a chromium/chromia bilayer architecture. Consisting of an internal 1 μm pure Cr layer and the optimized external chromia scale, this configuration was designed to combine the advantages of inert-ceramic and metallic coatings in the aggressive, low-oxygen liquid metal environment.
Accordingly, the research is pursued through a two-step approach:

- **Characterize the thermal oxidation kinetics:** Perform a fundamental investigation into the high-temperature structural evolution of HiPIMS-deposited metallic chromium to evaluate the intrinsic microstructural properties of the thermally grown Cr_2O_3 scales. Subsequently, exploit the findings of this characterization to select the optimal thermal oxidation parameters for the final barrier design.
- **Validate the corrosion performance in liquid lead:** Evaluate the protective efficacy of the optimized bi-layer architecture, and identify its underlying degradation mechanisms, through the exposure in an LFR-relevant stagnant liquid lead pool.

2. Methods

2.1. Production and Oxidation of Chromium Thin Films

Highly compact, 1 μm-thick pure metallic chromium films were deposited on monocrystalline silicon (for the oxidation campaign) and AISI 316L steel (for corrosion tests) via High-Power Impulse Magnetron Sputtering (HiPIMS). To ensure maximum film density and adhesion, optimized parameters (150 V pulsed bias, 100 μs pulse length) were applied. Subsequently, controlled thermal annealing was performed in an electric muffle furnace in air.

2.2. Characterization Techniques

Pristine, oxidized, and corroded specimens were evaluated using a comprehensive multimodal approach: Scanning Electron Microscopy (SEM) to assess planar morphology and cross-sectional scale thickness; Energy Dispersive X-Ray Spectroscopy (EDXS) for quantitative elemental mapping; multi-wavelength Raman spectroscopy (457, 514, and 660 nm) to confirm the phase purity of the Cr_2O_3 scale, evaluate macroscopic residual stresses, and identify post-exposure corrosion products; and Photoluminescence (PL) spectroscopy to qualitatively probe the concentration of bulk point defects within the oxide lattice.

2.3. Corrosion Tests

Liquid metal exposure was conducted in the CAPSULE facility at the ENEA Brasimone research center. Coated AISI 316L specimens were immersed in stagnant liquid lead at 600 °C for 1000 h, with dissolved oxygen controlled at 10^{-7} wt% to replicate LFR core conditions. Post-exposure, to isolate true degradation mechanisms from handling artifacts, a comparative approach was adopted: for each tested configuration, one sample was chemically washed to dissolve adhered lead, while a duplicate was left unwashed. Finally, specimens were cross-sectioned and embedded in resin for microstructural analysis.

3. Results and discussion

3.1. Characterization of thermally grown chromia

Building on previous findings by the NanoLab research group, an experimental annealing campaign was set up to characterize the thermally grown oxide scales on HiPIMS-deposited metallic chromium thin films. Specifically, the specimens were annealed in air at temperatures of 500 °C, 550 °C, and 600 °C for dwell times of 1 h, 3 h, 5 h, and 10 h.
The morphological characterization confirmed that the thermal oxidation process successfully produced continuous, dense, and firmly adherent corundum-phase Cr_2O_3 scales (as shown in Fig. 1). The images highlight the significant grain coarsening and barrier thickening driven by extended thermal exposure.

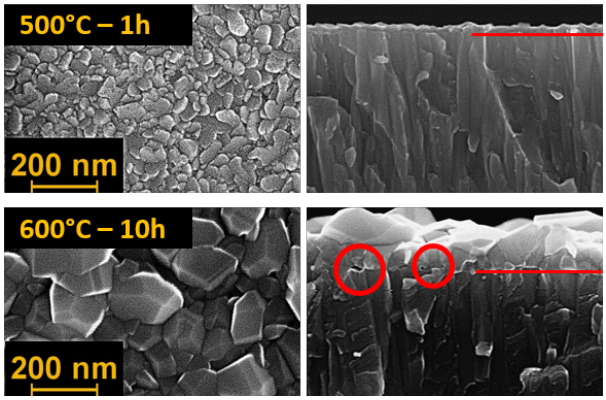

Figure 1: Planar (left) and cross-sectional (right) SEM micrographs of the Cr_2O_3 scales grown at 500 °C for 1 h (top) and 600 °C for 10 h (bottom). Red circles indicate the nanovoids at the chromia-chromium interface.

The thickness evolution is consistent with a parabolic growth law, characteristic of an ionic diffusion-driven process. Both scale thickness and grain size increased with thermal exposure, coarsening from approximately 40 nm (500 °C, 1 h) up to 95 nm, and reaching a maximum thickness of 125 nm after 10 hours at 600 °C. As a consequence of grain size growth, the surface of the oxide became more 3D with multifaceted grains, and surface roughness increased as annealing conditions became harsher. While the grown oxide layers remained highly dense, prolonged oxidation under the harshest condition (600 °C for 10 hours) led to the formation of localized nanovoids at the oxide-chromium interface (circled in red in Fig. 1). These interfacial nanopores are attributed to the thermally driven migration and coalescence of vacancies, acting as a structural healing mechanism for the bulk crystal lattice [4].

Multi-wavelength Raman spectroscopy confirmed the phase purity of the Cr_2O_3 oxide across all tested regimes. Notably, utilizing a 457 nm laser triggered a strong Resonance Raman effect, associated with a specific d-d electronic transition of Cr^{3+} ions. This massive signal amplification proved crucial for characterizing ultra-thin (30 nm) scales. As shown in Figure 2, resonance selectively amplified the Cr-dominated E_g vibrational modes over the A_{1g} peak, compared to the non-resonant spectrum obtained with 514 nm excitation laser.

Additionally, a weaker near-resonance effect was observed using a 660 nm laser, driven by its energetic proximity to a secondary spin-forbidden transition.

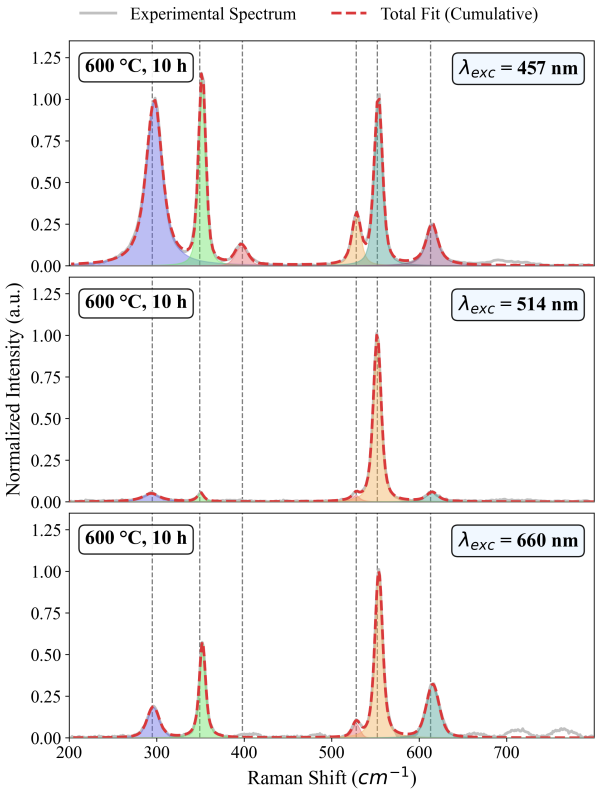

Figure 2: Deconvolution of the normalized Raman spectra acquired on the thermally grown Cr_2O_3 scale annealed at 600 °C for 10 h. The stacked plots illustrate the background-subtracted experimental data (solid gray line), the cumulative total fit (red dashed line), and the individual Raman-active vibrational modes (colored filled areas).

Furthermore, Raman spectroscopy was used for the estimation of residual stresses within the oxide scales [5]. Specifically, the macroscopic residual stress state was quantified by measuring the wavenumber displacement of the principal A_{1g} vibrational mode (centered at 552 cm^{-1}) relative to its stress-free bulk reference position. The stress evaluation indicated that all thermally grown scales exhibited a compressive residual stress state (ranging from -0.353 GPa to -1.055 GPa), which is expected to improve the fracture toughness of the ceramic layer. The data highlighted a significant stress relaxation at 600 °C between 1 and 5 hours likely associated to the activation of thermal creep.

Finally, photoluminescence (PL) spectroscopy

revealed an emission band centered at 1.66 eV, which may provide qualitative insights into the evolution of defect-related luminescent centers within the chromia lattice. The intensity of this band peaked after 5 hours at 600 °C but decreased significantly at 10 hours, as shown in Fig. 3. This drop is hypothesized to be the result of a structural healing mechanism, where prolonged thermal exposure promotes the migration and coalescence of isolated point defects at the interface, effectively reducing their concentration in the bulk oxide.

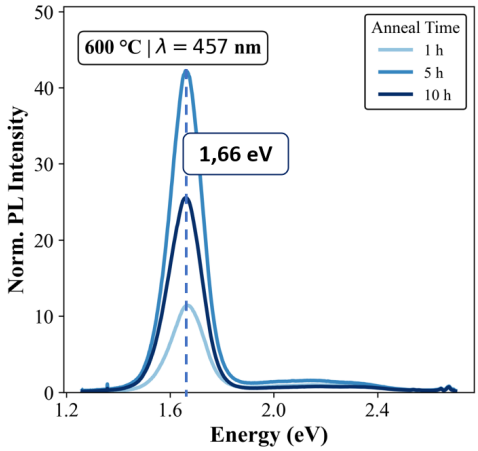

Figure 3: Photoluminescence (PL) spectra of the thermally grown chromia scales annealed at 600 °C for 1, 5, and 10 hours, collected using the 457 nm excitation wavelength.

This behavior is consistent with a hypothesized lattice healing mechanism: prolonged thermal exposure may promote the reduction of bulk defects by driving their migration and coalescence into localized nanometric voids, which were observed via SEM exclusively at the metal/oxide interface (Fig. 1). This process likely promotes the continuous incorporation of oxygen atoms to balance the oxide stoichiometry. Alongside this primary feature, excitation with a 660 nm laser revealed two additional, less intense PL bands, suggesting the presence of multiple localized defect states within the crystal lattice.
In conclusion, HiPIMS-deposited chromium thin films successfully develop dense, high-quality Cr_2O_3 scales under high-temperature oxidation. Furthermore, the implementation of multi-wavelength resonant Raman spectroscopy of chromium oxides provided a powerful, non-destructive approach to probe the phase structure and gain insights into the electronic properties of these ultra-thin barriers. These findings establish the scientific foundation for the subsequent research phase.

3.2. Corrosion performance in liquid lead

Drawing upon the fundamental microstructural insights obtained during the preliminary thermal treatments, two promising bilayer configurations were selected: Coating-Chromia-5 (annealed at 600 °C for 5 hours) and Coating-Chromia-10 (annealed at 600 °C for 10 hours). These annealing conditions were selected to optimize the protective barrier; they provide a sufficient oxide thickness (100–125 nm) and a moderate compressive residual stress to mitigate fracture, potentially facilitating a process of structural relaxation and defect annihilation within the chromia lattice. These architectures were replicated on AISI 316L austenitic stainless steel, selected as the reference structural material for LFR core components. To assess the performance of these coatings in an LFR-relevant environment, the bilayer configurations were tested as described in Section 2.3.
To accurately reconstruct the degradation mechanisms and isolate true corrosion phenomena from handling artifacts, both chemically washed and unwashed samples were analyzed. Furthermore, the uncoated rear surface of the Coating-Chromia-10 sample was analyzed to benchmark protective efficacy. Although pre-oxidized during the identical 10-hour thermal oxidation, its native scale proved entirely insufficient. The bare steel suffered massive degradation, exhibiting 10 μm deep pits and severe nickel depletion. Post-exposure characterization revealed a stark divergence in the performance of the two configurations. Coating-Chromia-5 demonstrated inadequate protection, suffering a complete structural breakdown. The barrier failed to protect the underlying substrate, allowing inward penetration of liquid lead. This infiltration drove a severe outward dissolution of nickel and generated corrosion pits up to 3 μm in width across the steel surface. The severely degraded planar morphology of the post-exposure substrate is depicted in Fig. 4a.
Conversely, Coating-Chromia-10 provided a significant enhancement in the system's corrosion resistance. While the barrier arrested macro-

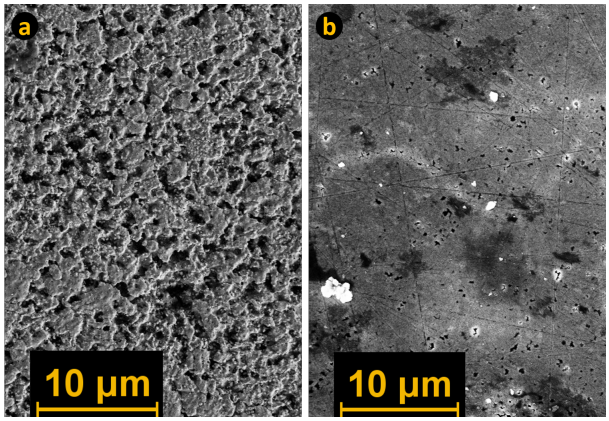

Figure 4: Planar SEM micrographs of the chemically washed specimens after 1000 hours of exposure to stagnant liquid lead at 600 °C: (a) Coating-Chromia-5; and (b) Coating-Chromia-10.

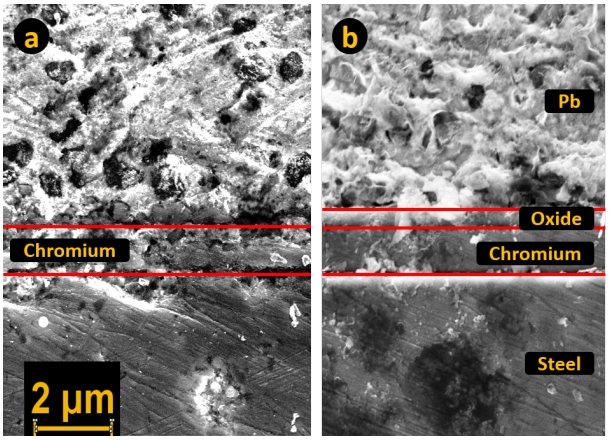

Figure 5: Cross-sectional SEM micrographs of the post-exposure unwashed specimen: (a) Coating-Chromia-5, revealing the total degradation of the protective barrier and massive inward penetration of lead into the underlying substrate; and (b) Coating-Chromia-10, showing the preservation of the thickened oxide scale.

scopic Pb infiltration, it did not fully impede the outward elemental diffusion from the substrate. Steel alloying elements, namely Fe, Ni, and Mn, migrated through the scale to form mixed Fe-Cr spinels (identified through Raman spectroscopy) or dissolve into the lead, leaving localized nanopits on the underlying steel (visible in the planar SEM micrograph in Fig. 4b). The cross-sectional EDXS data for the unwashed Coating-Chromia-10 sample (Fig. 6) suggest that the original bilayer structure remained intact and that macroscopic infiltration of lead into the steel substrate did not occur, within the resolution limits of the analysis. Cross-sectional SEM imaging (reported in Fig. 5b) revealed that the oxide scale thickened significantly during the 1000-hour exposure, increasing from 125 nm to approximately 516 nm. This suggests that chromium from the underlying metallic layer, along with substrate alloying elements, likely diffused outward to react with the dissolved oxygen.

Crucially, the comparison between cross-sectional SEM images reported in Fig. 5 highlights the stark divergence in the structural evolution of the two coatings.

This marked difference in corrosion resistance is likely attributable to the microscopic defect chemistry and thermodynamic stability of the initial oxides, rather than their physical thickness or macroscopic morphology. It is hypothesized that the extended 10-hour pre-oxidation treatment provided sufficient thermal energy and exposure to the oxidizing environment to heal the chromia lattice, reducing the concentration of bulk point defects. In contrast, the higher density of unhealed point defects in the 5-hour sample may be associated with fast-diffusion pathways, facilitating the rapid inward penetration of the heavy liquid metal and the subsequent structural degradation.

Nevertheless, despite the superior barrier properties of the mature 10-hour scale, both the coatings ultimately failed due to severe interfacial delamination at the chromium-steel boundary. Based on post-exposure morphological evidence, this massive detachment is hypothesized to have occurred during the cooling and solidification phase of the liquid lead. Because the highly wettable chromia surface likely established a strong bond with the surrounding lead, the severe thermal contraction stresses generated as the heavy metal solidified may have mechanically torn the entire protective architecture away from the underlying substrate. This chronological interpretation is supported by the observation that, even in regions where the detachment is most pronounced, there is no trace of lead directly wetting the exposed steel surface, nor are there any signs of localized corrosion on the bare substrate.

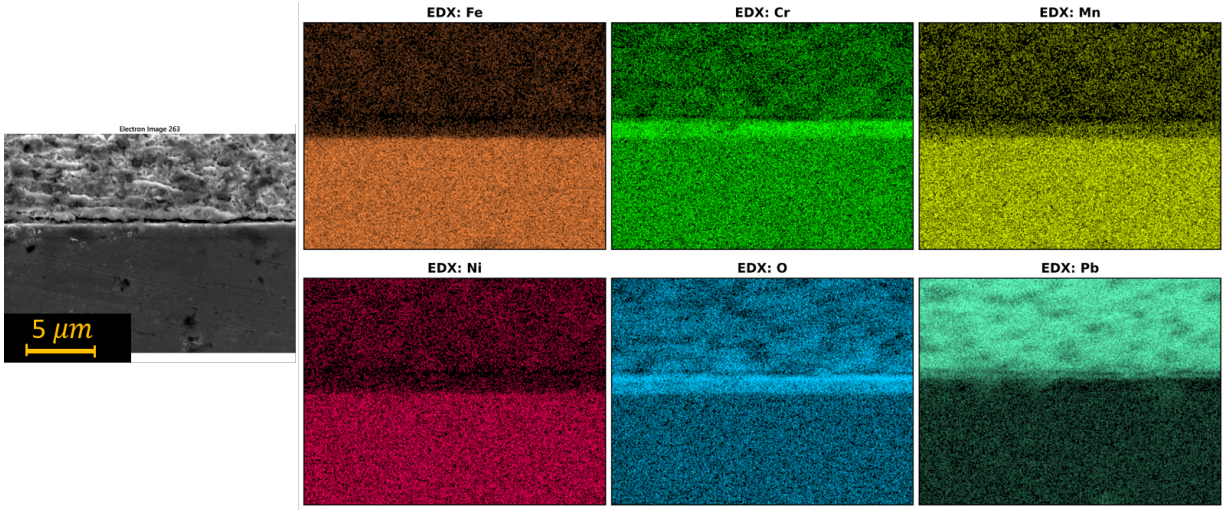

Figure 6: Cross-sectional EDXS elemental mapping of the unwashed Coating-Chromia-10 sample, demonstrating the preservation of the chromium/chromia bilayer and the complete absence of lead (Pb) penetration into the steel substrate.

4. Conclusions

This experimental work provides fundamental insights into the oxidation mechanisms of HiPIMS-deposited metallic chromium coatings and their degradation behavior in LFR-relevant environments. This work identifies some critical drivers of anticorrosive performance.

The study yielded three key findings:

- **Optimization of the Oxide Scale:** The study confirms that thermal annealing of HiPIMS-deposited chromium is a viable strategy for growing dense, homogeneous Cr_2O_3 scales. Notably, longer annealing times at higher temperatures consistently produce thicker oxides with superior crystalline quality, larger grains and rougher surface.
- **Assessment of Barrier Efficacy:** Experimental results suggest a potential correlation between the initial microstructural maturity of the Cr_2O_3 layer and its protective capability. A more mature oxide scale seems to mitigate ions diffusion pathways, which may reduce the barrier's vulnerability to inward lead penetration and outward elemental diffusion.
- **Critical Challenges and Methodological Insights:** Despite the proven protective potential of mature chromia scales, outward elemental migration and interfacial delamination remain significant hurdles. Furthermore, this work demonstrates that post-exposure chemical cleaning must be rigorously calibrated as aggressive washing procedures can alter the post-exposure analysis.

In conclusion, this research provides a scientific basis for developing chromium-based anticorrosive barriers. Future work must go beyond simple oxide growth, focusing on refining annealing parameters to better balance crystalline maturity with mechanical stability. Addressing the persistent challenges of interfacial adhesion and thermomechanical compatibility will also be essential to meet the operational requirements of Generation IV nuclear systems.

References

[1] Gong, X., et al., Environmental degradation of structural materials in liquid lead- and lead-bismuth eutectic-cooled reactors, *Progress in Materials Science*, 2022.

[2] Song, H., et al., Chromium-based coatings and diffusion barriers for accident-tolerant fuel applications, *Journal of Materials Science*, 2026.

[3] Wang, L., et al., Corrosion behavior of Cr coating on ferritic/martensitic steels in liquid lead-bismuth eutectic at 600 °C and 700 °C, *Journal of Materials Research and Technology*, 2024.

[4] Auguste, R., et al., A multimodal approach to re-visiting oxidation defects in Cr_2O_3, *npj Materials Degradation*, 2022.

[5] Kemdehoundja, M., et al., Growth stresses in α-Cr_2O_3 thermal oxide films determined by in situ high temperature Raman spectroscopy, *Journal of Applied Physics*, 2007.